Princeton Plasma Physics Laboratory

Development of Variational Guiding Center Algorithms for Parallel Calculations in Experimental Magnetic Equilibria

C. Leland Ellison, J.M. Finn,
H. Qin, W.M. Tang

October 2014

PRINCETON
PLASMA PHYSICS
LABORATORY

Princeton Plasma Physics Laboratory
Report Disclaimers

Full Legal Disclaimer

Trademark Disclaimer

PPPL Report Availability

Princeton Plasma Physics Laboratory:

http://www.pppl.gov/techreports.cfm

Office of Scientific and Technical Information (OSTI):

http://www.osti.gov/scitech/

Related Links:

U.S. Department of Energy

Office of Scientific and Technical Information

Development of variational guiding center algorithms for parallel calculations in experimental magnetic equilibria

C. Leland Ellison[1], J. M. Finn[2], H. Qin[1,3], W. M. Tang[1]

[1]*Princeton Plasma Physics Laboratory, Princeton, NJ, 08550 USA*

[2]*Los Alamos National Laboratory, Los Alamos, NM 87545, USA and*

[3]*Department of Modern Physics, University of Science*
and Technology of China, Hefei, Anhui 230026, China

Abstract

Structure-preserving algorithms obtained via discrete variational principles exhibit strong promise for the calculation of guiding center test particle trajectories. The non-canonical Hamiltonian structure of the guiding center equations forms a novel and challenging context for geometric integration. To demonstrate the practical relevance of these methods, a prototypical variational midpoint algorithm is applied to an experimental magnetic equilibrium. The stability characteristics, conservation properties, and implementation requirements associated with the variational algorithms are addressed. Furthermore, computational run time is reduced for large numbers of particles by parallelizing the calculation on GPU hardware.

I.   INTRODUCTION

One of the principle challenges of plasma physics is to accurately model multi-scale phenomena. As magnetically-confined fusion plasmas progress toward the burning plasma regime, the largest characteristic temporal and spatial scales grow increasingly disparate from the smallest. For instance, the gyro-orbits exhibited by electrons in ITER will occur at a timescale thirteen orders of magnitude faster than the pulse discharge length. Numerically modeling test particle dynamics in burning plasma devices thus presents a formidable challenge. The analytic guiding center transformation partially mitigates this challenge by shifting the shortest characteristic timescale from the gyroperiod to the toroidal transit time. However, modeling the dynamics of fast particles such as runaway electrons and hot alphas still requires resolving tens of thousands of toroidal transits. The numerical computation of such long term dynamics stands to benefit from advances in algorithms and computational hardware.

On the numerical analysis front, so-called "geometric" algorithms retain physically conserved quantities in the discrete flow, resulting in excellent long term numerical fidelity [1]. An algorithm that conserves energy or momentum more accurately represents the physical system after many numerical time advances than an algorithm that conserves no such quantities. In essence, while truncation error is unavoidable in any numerical approximation, numerically conserved quantities force the errors to manifest in relatively benign features, such as in the phase of a periodic trajectory. The importance of magnetically-confined fast particle dynamics makes the calculation of guiding center trajectories an appealing candidate for application of structure preserving algorithms.

Moreover, the guiding center equations of motion are an especially novel context for geometric integration because the most natural description of the dynamics is non-canonically Hamiltonian [2, 3]. From a geometric perspective, the structure of Hamilton's equations is independent of the coordinates used to represent them [4, 5]. However, most structure-preserving numerical methods rely on representing Hamilton's equations in canonical coordinates [1]. The task of developing numerical methods that preserve the structure of non-canonical Hamilton's equations remains an outstanding challenge in the field of numerical analysis [1, 6]. While the guiding center equations of motion may be cast in canonical coordinates [3, 7, 8], a global transformation may not exist for arbitrary magnetic geome-

try, and local transformations may be undesirably complex for magnetic configurations of interest [9].

One technique for constructing algorithms ensures the presence of conserved quantities by discretizing the variational principle that underlies the equations of motion [10]. By requiring the discrete trajectory to extremize a discrete action, the numerical time advance inherits the conservation properties of the continuous dynamics. Such an approach has proven insightful for the analysis of familiar symplectic algorithms [10] while yielding novel schemes unlikely to arise from direct discretization of the equations of motion [11–13]. The success of variational algorithms motivated studies in discretizing the guiding center Lagrangian, where test cases in simple magnetic geometry exhibited the characteristic long-term numerical fidelity [14–18].

In this article, algorithms derived from a discrete variational principle are discussed as promising methods for the structure-preserving integration of guiding center test particle trajectories. Expanding upon the early positive results, good long-term numerical fidelity has now been observed in magnetic fields interpolated from experimental equilibria. Moreover, the variational algorithms have been implemented on general-purpose graphics processing units using the CUDA programming language, and excellent scaling to large numbers of particles obtained. The challenges associated with using variational guiding center algorithms are also explicated. In particular, the multistep characteristics of the resulting algorithms complicate interpretation of the conserved quantities and require careful initial condition selection. An additional implementation consideration is the extraction of the vector potential from the numerical magnetic equilibria. The observed long-term numerical fidelity motivates ongoing development, particularly the pursuit of variational discretizations that may further ameliorate the drawbacks of the present generation of variational guiding center algorithms.

II. BACKGROUND

To establish context for the variational guiding center algorithms, this section reviews guiding center dynamics, symplectic integration, and variational integration. Given the inter-disciplinary nature of this work, it is helpful to summarize foundational elements of the plasma physics, classical mechanics, and numerical analysis components. In discussing the

guiding center coordinate transformation, emphasis is placed on understanding the resulting equations of motion as a Hamiltonian system in non-canonical coordinates. Symplectic integrators are then described as numerical methods that produce trajectories along solutions of a Hamiltonian system nearby to the original being modeled. Variational integrators may then be understood as a systematic means of deriving symplectic algorithms, given appropriate properties of the Lagrangian governing the dynamics.

A. Hamiltonian Guiding Center Dynamics

A prominent technique for reducing the complexity of magnetized charged particle dynamics is the transformation to guiding center coordinates [2, 3]. If the scale length over which the electric and magnetic fields vary is much longer than the radius at which a charged particle orbits a magnetic field line, the dynamics are approximately invariant with respect to the phase of the particle's gyro-orbit. Analytically, transforming to coordinates in which this invariance is manifest reduces the dimensionality of the dynamics from six dimensions to four. Numerically, one no longer needs to resolve the rapid gyromotion while tracking the guiding center of the particle orbit along and across magnetic field lines.

Starting with a charged particle in electric and magnetic fields, the guiding center transformation is an approximate transformation from the original charged particle position $\mathbf{q}$ and velocity $\mathbf{v}$ to the position of the guiding center $\mathbf{x}$ and three additional variables (u, μ, Θ). Here, u is the velocity of the guiding center along the magnetic field line, μ is the magnetic moment, and Θ is the gyrophase, which is the angle of the gyro-orbit with respect to some initial position. In the new coordinates, the Θ, μ dynamics decouple from the other components and may be ignored if only the guiding center position and velocity are of interest.

To determine the equations of motion in the guiding center coordinates $(\mathbf{x}, u, \mu, \Theta)$, one turns to the origin of the equations of motion for a charged particle in a magnetic field. To describe the charged particle dynamics, one typically resorts to a Lagrangian formalism or a Hamiltonian formalism. Understanding the relationship between these two descriptions is crucial to understanding the particular form of the guiding center Lagrangian and the novelty of structure-preserving algorithms in this context. The following discussion highlights the relevant details found in Reference [3].

From the Lagrangian perspective, one may derive the familiar Lorentz force law starting

4

from the charged particle Lagrangian:

$$L(\mathbf{q}, \dot{\mathbf{q}}) = \frac{1}{2}m|\dot{\mathbf{q}}|^2 + \frac{e}{c}\mathbf{A} \cdot \dot{\mathbf{q}} - e\phi. \tag{1}$$

Here, $\dot{\mathbf{q}} = \frac{d\mathbf{q}}{dt}$, m is the mass of the particle, e is the charge, $\mathbf{A}$ is the vector potential and ϕ is the scalar potential. For the purposes of this discussion, we deem this Lagrangian a "configuration-space Lagrangian", as it acts on points $(\mathbf{q}, \dot{\mathbf{q}})$ in the tangent bundle TQ of the configuration space Q [4]. Given a path $\mathbf{q}(t)$ with $t \in [0, T] \subset \mathbb{R}$, the action integral is given by:

$$S(\mathbf{q}(t)) = \int_0^T L(\mathbf{q}(t), \dot{\mathbf{q}}(t))dt. \tag{2}$$

Requiring the action to be extremized with respect to arbitrary path variations $\delta\mathbf{q}$, one finds the Euler-Lagrange equations for a charged particle:

$$dS \cdot \delta\mathbf{q} = 0 \quad \Rightarrow$$
$$m\ddot{\mathbf{q}} = e\mathbf{E} + \frac{e}{c}\dot{\mathbf{q}} \times \mathbf{B}. \tag{3}$$

Here we see the electric field $\mathbf{E} = -\nabla\phi$ and the magnetic field $\mathbf{B} = \nabla \times \mathbf{A}$.

Instead of a second order differential equation in three variables, we may describe the dynamics using first order equations in six variables by turning to the Hamiltonian perspective. The Hamiltonian for a charged particle is given by:

$$H(\mathbf{q}, \mathbf{p}) = \frac{1}{2m}|\mathbf{p} - \frac{e}{c}\mathbf{A}|^2 + e\phi, \tag{4}$$

where $\mathbf{p} = m\dot{\mathbf{q}} + \frac{e}{c}\mathbf{A}$. The equations of motion are given by Hamilton's canonical equations:

$$\dot{\mathbf{q}} = \frac{\partial H}{\partial \mathbf{p}} \qquad \dot{\mathbf{p}} = -\frac{\partial H}{\partial \mathbf{q}}. \tag{5}$$

These two formulations offer equivalent descriptions of the dynamics while exhibiting different flexibility in their potential for coordinate transformations. From the Lagrangian perspective, one is free to transform the three configuration coordinates q^i; extremizing the action with respect to perturbations in the new coordinates recovers the proper dynamics. However, the velocity variables $\dot{q}^i$ are directly determined as the time derivatives of the configuration coordinates, thereby restricting the ability to transform the velocity coordinates. Alternatively, the Hamiltonian description elevates the momenta p_i to equal status as the configuration coordinates q^i. However, transformations on the six variables $(\mathbf{q}, \mathbf{p}) \mapsto (\mathbf{Q}, \mathbf{P})$

must retain the canonical structure of Hamilton's equations. Otherwise, one must consider how the Poisson bracket transforms, which is a less straightforward task than the variational principle utilized in the Lagrangian context. Neither of these two formalisms offers the desired freedom of transforming from physical charged particle coordinates $(\mathbf{q}, \mathbf{v})$ to the guiding center coordinates $(\mathbf{x}, u, \mu, \Theta)$.

A hybrid approach facilitates the calculation of Hamiltonian equations in general coordinates utilizing an action principle in phase space [19, 20]. Given phase-space coordinates $(\mathbf{q}, \mathbf{p})$, consider the "phase-space Lagrangian" given by:

$$L(\mathbf{q}, \mathbf{p}, \dot{\mathbf{q}}, \dot{\mathbf{p}}) = \mathbf{p} \cdot \dot{\mathbf{q}} - H(\mathbf{q}, \mathbf{p}). \tag{6}$$

This expression for the Lagrangian is numerically equivalent to that given by the Legendre transform, but here $\mathbf{q}$ and $\mathbf{p}$ are retained as independent coordinates. Extremizing the action integral of this Lagrangian with respect to arbitrary path variations $(\delta\mathbf{q}, \delta\mathbf{p})$, one recovers Equation (5) as the "Euler-Lagrange equations". By deriving Hamilton's equations from a variational principle, arbitrary transformation of the six phase-space coordinates may be performed and determining the dynamics in the new coordinates involves application of the familiar variational principle.

This phase-space Lagrangian is the starting point for the transformation to guiding center coordinates. One manipulates the charged particle phase-space Lagrangian, neglecting small terms in the mass-to-charge ratio. The resulting guiding center Lagrangian is given by:

$$L(\mathbf{x}, u, \mu, \Theta, \dot{\mathbf{x}}, \dot{u}, \dot{\mu}, \dot{\Theta}) =$$
$$\left(\frac{e}{mc}\mathbf{A} + u\mathbf{b}\right) \cdot \dot{\mathbf{x}} + \frac{c}{e}\mu\dot{\Theta} - \left(\frac{u^2}{2} + \mu B + \frac{e}{m}\phi\right), \tag{7}$$

where $\mathbf{b}$ is the magnetic field unit vector and B the magnetic field magnitude. We emphasize that this Lagrangian originates from Equation (6), not the charged particle Lagrangian Equation (1). In resemblance to the canonical phase-space Lagrangian of Equation (6), the guiding center Lagrangian is linear in the velocities $(\dot{\mathbf{x}}, \dot{u}, \dot{\mu}, \dot{\theta})$, and includes the guiding center Hamiltonian:

$$H_{gc}(\mathbf{x}, u, \mu, \Theta) = \frac{u^2}{2} + \mu B + \frac{e}{m}\phi. \tag{8}$$

The action of the guiding center Lagrangian is extremized with respect to variations

$(\delta \mathbf{x}, \delta u, \delta \mu, \delta \Theta)$ by paths satisfying the following first order ODE system:

$$\left(A^\dagger_{i,j} - A^\dagger_{j,i}\right)\dot{x}^i - \left(\mu B_{,j} + \frac{e}{m}\phi_{,j}\right) = 0 \qquad j = 1, 2, 3$$

$$u - b_i \dot{x}^i = 0$$

$$\dot{\mu} = 0$$

$$\dot{\Theta} - \frac{eB}{mc} = 0 \tag{9}$$

Here, $\mathbf{A}^\dagger = \frac{e}{mc}\mathbf{A} + u\mathbf{b}$, summation over repeated indices is implied, and indices appearing after a comma denote differentiation with respect to the corresponding component. As desired from the onset of the guiding center transformation, the (μ, Θ) dynamics decouple from the $(\mathbf{x}, u)$ dynamics. Henceforth, μ will be treated as constant and the gyrophase Θ ignored.

Upon inspection of the guiding center Equations (9), it is clear the ODE system does not have the canonical Hamiltonian form of Equations (5). Indeed, they were obtained via an action principle in phase space following a non-canonical coordinate transformation. While Equations (5) are the familiar setting for discussing Hamiltonian dynamics, Hamilton's equations may defined more generally as:

$$\Omega_{ij}\dot{z}^i = H_{,j}, \tag{10}$$

where Ω is a non-degenerate anti-symmetric matrix. The canonical case of Equation (5) may be viewed as a specific case of Equation (10) in which $\mathbf{z} = (\mathbf{q}, \mathbf{p})$ and $\Omega = \begin{bmatrix} 0 & I \\ -I & 0 \end{bmatrix}$. The guiding center equations are also in the form of Equation (10) with $\mathbf{z} = (\mathbf{x}, u)$ and

$$\Omega = \begin{bmatrix} 0 & B^\dagger_3 & -B^\dagger_2 & -b_1 \\ -B^\dagger_3 & 0 & B^\dagger_1 & -b_2 \\ B^\dagger_2 & -B^\dagger_1 & 0 & -b_3 \\ b_1 & b_2 & b_3 & 0 \end{bmatrix}, \tag{11}$$

where $\mathbf{B}^\dagger = \nabla \times \mathbf{A}^\dagger$. It is in this sense that the four-dimensional guiding center equations are considered non-canonically Hamiltonian.

B. Symplectic Integration

For the numerical integration of Hamilton's Equations (5), a class of algorithms known as as symplectic integrators display excellent long-term numerical fidelity [1]. The discrete numerical advances of symplectic algorithms share a central property with exact solutions to Hamilton's equations; they preserve a symplectic structure. In fact, numerical trajectories generated by symplectic algorithms lie asymptotically near exact solutions to a Hamiltonian system that converges to the original as the numerical step size tends to zero. As a consequence, important metrics like energy error remain bounded by some small number for exponentially long simulation times. Leveraging the properties of symplectic algorithms is therefore a powerful tool for obtaining good numerical behavior after many time steps when the dynamical system of interest is Hamiltonian.

A map Φ is symplectic when the pullback of the symplectic structure by Φ is equivalent to the original symplectic structure. Precisely, a Hamiltonian system is defined by a symplectic manifold (M, Ω) and a Hamiltonian function H. A map $\Phi : M \to M$ is symplectic when:

$$\Omega = \Phi^* \Omega, \tag{12}$$

where Φ^* is the pullback. The maps we'll be considering in this work will all be time advance maps. That is, Φ will be the solution to a differential equation specified in terms of a vector field or it will be the solution to a numerical update rule.

For an intuitive understanding of the symplecticity condition Equation (12), recall that symplectic structures are operators acting on pairs of tangent vectors to yield real numbers [1, 5, 21]. For instance, the canonical symplectic structure defined in Sec. (II A) determines the oriented area spanned by a pair of tangent vectors in phase space. In this canonical context, one checks whether a map Φ is symplectic by advancing a pair of test vectors along Φ and checking whether the area spanned by the new vectors is equivalent to the original area. This is the essence of the pullback in Equation (12); in effect, one calculates the new vectors according the calculus chain rule [5].

The symplecticity of maps is central to Hamiltonian mechanics because flows of Hamiltonian vectors fields are symplectic. In the canonical context, solutions to Hamilton's equations are area preserving. More generally, suppose the time-t flow map ϕ_t satisfying:

$$\frac{d\phi_t}{dt} = X_H(\mathbf{z}(t)), \tag{13}$$

8

where the Hamiltonian vector field X_H is defined by $X_H = \dot{\mathbf{z}}$ in Equation (10). The flow map ϕ_t satisfies the symplecticity condition Equation (12) for all t, as is shown in many standard references [1]. So, solutions of Hamilton's equations are symplectic.

Conversely, a numerical trajectory generated using a symplectic algorithm lies asymptotically near the exact solution of *some* Hamiltonian system. In practice, this means a discrete trajectory $\{\mathbf{z}_k\}_{k=0}^N$ generated by a symplectic numerical algorithm is indistinguishable from a discrete sampling of a continuous solution to Hamiltonian equations for some Hamiltonian $\widetilde{H}$. Because the numerical trajectory is the flow of a Hamiltonian system that is close to the original for small h, the numerical trajectory will strongly resemble the true solution. In particular, the numerical energy will differ from the original by $\widetilde{H} - H$ for exponentially long times [1].

This result is obtained by performing a backward error analysis. Given a numerical method $\varphi_h(\mathbf{z}_k) = \mathbf{z}_{k+1}$ with numerical step size h, one presumes the existence of a continuous flow map $\widetilde{\varphi}_t$ such that $\widetilde{\varphi}_{t=kh} = \varphi_h^k$. That is, backward error analysis seeks a continuous system whose solution sampled at discrete times exactly matches the discrete numerical trajectory. Insight may then be gained by comparing the vector field governing the backward error dynamics to the original vector field. In detail, one supposes $\widetilde{\phi}_t$ satisfies:

$$\frac{d\widetilde{\phi}_t}{dt} = \tilde{X} = X_0 + hX_1 + h^2 X_2 + ..., \tag{14}$$

where the X_i may be determined from the numerical update rule and $X_0 = X_H$ must hold for consistent algorithms. If the numerical map φ_h is symplectic, it can be shown that the X_i are Hamiltonian [1], so

$$\Omega_{ij}\widetilde{X}^i = \widetilde{H}_{,j} \tag{15}$$

with $\widetilde{H} = H + hH_1 + ...$ In general, the series in Equation (14) is asymptotic and must be truncated at optimal order for specific values of numerical step size h.

Much of the literature on symplectic integrators focuses on Hamiltonian systems written in canonical form, as in Equation [5]. However, several important systems possess the more general Hamiltonian structure of Equation [10], and may be difficult to cast in canonical form. Examples of non-canonical Hamiltonian systems include magnetic field line flow [22] and guiding center dynamics [2, 3]. In these settings, preservation of the non-canonical symplectic structure governing the Hamiltonian dynamics is desirable to obtain numerical

trajectories with good long term behavior. In specific cases, this has been achieved, but general non-canonically symplectic numerical methods are not known [6].

C. Variational Integration

Additional insight regarding symplectic algorithms can be found in discrete variational principles [10]. The conventional setting for discussing symplectic numerical methods refers to modeling Hamilton's equations. However, just as a complimentary description of the continuous dynamics resides in the Lagrangian formalism, symplectic integrators may be understood as resultant from discrete variational principles. In brief, all symplectic maps may be constructed from generating functions, and discretizing the Lagrangian action principle is a systematic means of constructing a generating function for a symplectic numerical time-advance map.

Suppose, for instance, a configuration space Lagrangian $L(\mathbf{q}, \dot{\mathbf{q}})$ with action given by Equation (2) and Euler-Lagrange equations:

$$\frac{\partial L}{\partial \mathbf{q}} - \frac{d}{dt}\frac{\partial L}{\partial \dot{\mathbf{q}}} = 0. \tag{16}$$

If the Lagrangian is regular, i.e. $\frac{\partial^2 L}{\partial \dot{\mathbf{q}}^2}$ is non-degenerate, then a unique path $\mathbf{q}(t)$ extremizes the action integral. From this, we define a discrete Lagrangian as an approximation to a small interval of the action:

$$L_d(\mathbf{q}_k, \mathbf{q}_{k+1}) \approx \int_{t_k}^{t_{k+1}} L(\mathbf{q}(t), \dot{\mathbf{q}}(t))dt, \tag{17}$$

where $\mathbf{q}(t)$ in the integrand is the unique trajectory extremizing the action integral with endpoints (t_k, t_{k+1}). A discrete action corresponding to a particular choice of discrete Lagrangian is identified as:

$$S_d(\mathbf{q}_0, ..., \mathbf{q}_N) = \sum_{k=0}^{N-1} L_d(\mathbf{q}_k, \mathbf{q}_{k+1}). \tag{18}$$

Variation of the action with respect to $\delta\mathbf{q}_k$ for arbitrary k yields the "discrete Euler-Lagrange equations":

$$dS_d \cdot \delta\mathbf{q}_k = 0 \Rightarrow$$

$$D_2 L_d(\mathbf{q}_{k-1}, \mathbf{q}_k) + D_1 L_d(\mathbf{q}_k, \mathbf{q}_{k+1}) = 0, \tag{19}$$

10

where the slot derivative D_i denotes differentiation with respect to the i-th argument. The discrete Euler-Lagrange Equations (19) are a numerical method for approximating solutions to the continuous Euler-Lagrange Equations (16). Simple choices for the discrete Lagrangian can yield familiar algorithms, such as the Störmer-Verlet method [10].

The variationally-derived discrete Euler-Lagrange equations may be formulated as a canonically symplectic map for the solution of Hamilton's Equations (5). The identification of a symplectic map follows from defining a "discrete Legendre transform":

$$\mathbf{p}_k = -D_1 L_d(\mathbf{q}_k, \mathbf{q}_{k+1})$$
$$\mathbf{p}_{k+1} = D_2 L_d(\mathbf{q}_k, \mathbf{q}_{k+1}). \tag{20}$$

These seemingly different definitions for the discrete momenta are equivalent for numerical trajectories satisfying the discrete Euler-Lagrange Equations (19). One may thus iterate Equations (20) as a numerical integrator for Hamilton's equations; symplecticity of the algorithm is a consequence of the discrete action principle [10]. Inspection of Equations (19) identifies the discrete Lagrangian L_d as a type-one generating function for the canonical transformation $(\mathbf{p}_k, \mathbf{q}_k)$ to $(\mathbf{p}_{k+1}, \mathbf{q}_{k+1})$, guaranteeing the numerical time advance will be symplectic.

III.   VARIATIONAL GUIDING CENTER ALGORITHMS

We turn now to the task of integrating the guiding center equations of motion Equation (9) in a structure-preserving manner. Ideally, a non-canonically symplectic algorithm could be constructed that preserves the guiding center symplectic structure Equation (11) in the sense of Equation (12). Given the non-canonical formulation, familiar symplectic algorithms such as symplectic Runge-Kutta methods are not directly applicable.

Inspired by the success of discretizing configuration-space action principles, recent work has developed guiding center algorithms by discretizing the guiding center Lagrangian Equation (7) [14–18]. Test problems in two spatial dimensions demonstrated excellent long-term numerical fidelity [14–16]. Here, we'll extend these results to experimental magnetic equilibria while describing the peculiarities that arise for variational guiding center algorithms. Because the guiding center Lagrangian originates from a non-regular phase-space Lagrangian, discretization yields different properties than those observed for the regular configuration-

space Lagrangians presumed in Section (II C). In particular, the methods are multistep algorithms for the integration of first-order differential equations, presenting initialization and stability considerations. An additional factor for the variational guiding center algorithms is the necessity of evaluating the magnetic vector potential in the numerical update rule.

A. Midpoint Discretization

The variational integrators literature offers many candidate discretization schemes for application to the guiding center Lagrangian [10–13]. As a representative example, we will primarily consider a midpoint discrete Lagrangian as in Reference [16]:

$$L_d(\mathbf{x}_k, u_{k+1/2}, \mathbf{x}_{k+1}) = A_i^\dagger \left(\frac{\mathbf{x}_k + \mathbf{x}_{k+1}}{2}, u_{k+1/2} \right) (x_{k+1}^i - x_k^i) - hH_{gc} \left(\frac{\mathbf{x}_k + \mathbf{x}_{k+1}}{2}, u_{k+1/2} \right), \tag{21}$$

where H_{gc} is given by Equation (8). The centered position evaluations are expected to yield a second-order accurate algorithm, and the absence of $\dot{u}$ in the guiding center Lagrangian allows staggering the u coordinate at half-integer times.

The discrete Euler-Lagrange equations corresponding to the midpoint discrete Lagrangian are given by:

$$\frac{1}{2}A_{i,j}^\dagger(k+1/2)[x_{k+1}^i - x_k^i] + \frac{1}{2}A_{i,j}^\dagger(k-1/2)[x_k^i - x_{k-1}^i] -$$
$$\left[A_j^\dagger(k+1/2) - A_j^\dagger(k-1/2) \right] - \frac{h}{2}[\mu B_{,j}(k+1/2) + \mu B_{,j}(k-1/2) +$$
$$\phi_{,j}(k+1/2) + \phi_{,j}(k-1/2)] = 0, \quad j = 1, 2, 3$$

$$b_i(k+1/2)[x_{k+1}^i - x_k^i] - hu_{k+1/2} = 0. \tag{22}$$

Here, factors of e and m have been normalized into the definitions of the fields and $(k+1/2)$ in the function evaluations indicates evaluation at $\left(\mathbf{x} = \frac{\mathbf{x}_k + \mathbf{x}_{k+1}}{2}, u = u_{k+1/2} \right)$, and $(k-1/2)$ is one time index earlier. These equations resemble the non-canonically Hamiltonian guiding center equations of motion written in the form of Equation (10).

The variational guiding center algorithm Equation (22) exhibits three features of interest: it is implicit, it is multistep, and the vector potential is evaluated. As an implicit algorithm,

implementation involves performing a nonlinear solve. In practice, Newton-Rhapson iterations typically converge within two to three iterations. One might strive for a discretization yielding an explicit variational algorithm, but the work of Reference [17] demonstrated that all explicit variational guiding center algorithms within a natural family of discrete Lagrangians were unstable. By multistep, we mean that Equation (22) depends on the previous two positions in time $(\mathbf{x}_{k-1}, \mathbf{x}_k)$ to determine the new position $(\mathbf{x}_{k+1})$. This may be expected from the form of the discrete Euler-Lagrange Equations (19), but is novel for integrating a first-order system of differential equations. Finally, the presence of the magnetic vector potential $\mathbf{A}$ will require constructing a vector potential from experimental equilibria specified in terms of the magnetic field $\mathbf{B}$.

B.   Multistep Characteristics

Multistep numerical methods possess several drawbacks in the context of structure-preserving algorithms that must be addressed and mitigated to successfully utilize the variational guiding center algorithms. From a stability perspective, multistep methods are well-known to exhibit parasitic modes [1, 23, 24]. These modes must remain small for the temporal simulation domain of interest. A related issue is that *linear* multistep methods cannot be symplectic in the conventional sense [25], and although Equation (22) is not a linear multistep method, it would be a surprising feature if it were symplectic in the sense of Equation (12).

Despite these drawbacks, the encouraging long-term behavior of the preliminary guiding center studies [14–16] suggests that the variational midpoint algorithm possesses desirable features nonetheless. This subsection endeavors to explain (and improve) the good behavior by investigating the parasitic modes present in the guiding center trajectories and establishing the presence of a conserved symplectic structure in the stable mode of the dynamics.

1.   Parasitic Modes

Multistep numerical algorithms admit parasitic modes, which are unphysical artifacts arising from the numerical dynamics occurring in a larger-dimensional space than that of the physical dynamics. The modes manifest as, for instance, even-odd oscillations in the

numerical trajectory. Ensuring the parasitic modes are smaller than the principle behavior is therefore important for successful application of multistep methods.

The presence of parasitic modes in the variational midpoint algorithm Equation (22) is demonstrated by performing an eigenvalue analysis. Letting $\mathbf{z} = (\mathbf{x}, u)^T$ and $\vartheta = (\mathbf{A}^\dagger, 0)$, the $h \to 0$ limit of the algorithm is given by:

$$\frac{1}{2}\vartheta_{i,j}\left(\frac{\mathbf{z}_0 + \mathbf{z}_1}{2}\right)(z_1^i - z_0^i) + \vartheta_j\left(\frac{\mathbf{z}_0 + \mathbf{z}_1}{2}\right) +$$
$$\frac{1}{2}\vartheta_{i,j}\left(\frac{\mathbf{z}_1 + \mathbf{z}_2}{2}\right)(z_2^i - z_1^i) - \vartheta_j\left(\frac{\mathbf{z}_1 + \mathbf{z}_2}{2}\right) = 0. \tag{23}$$

In the above, indices range from one to four and we have treated $u_{k+1/2}$ as $(u_k + u_{k+1})/2$ for simplicity and illustration. Linearizing about $\mathbf{z}_0$, we find:

$$\frac{1}{2}(\vartheta_{i,j}(\mathbf{z}_0) - \vartheta_{j,i}(\mathbf{z}_0))(z_2^i - z_0^i) = 0. \tag{24}$$

The non-degeneracy of the symplectic structure Ω ensures $\vartheta_{i,j} - \vartheta_{j,i}$ is invertible, and the ansatz that $\mathbf{z}_2 = \lambda\mathbf{z}_1 = \lambda^2\mathbf{z}_0$ yields the eigenvalue equation:

$$(\lambda^2 - 1)\mathbf{z}_0 = 0. \tag{25}$$

For our four dimensional system of interest, this yields four roots at $\lambda = 1$ and four at $\lambda = -1$. The behavior corresponding to the $\lambda = 1$ roots is referred to as the "principle mode", as it corresponds to a smooth trajectory in the $h \to 0$ limit [1, 23, 24]. The behavior at $\lambda = -1$ is referred to as the "parasitic mode", as the trajectory oscillates between even- and odd-numbered numerical time steps. Indeed, we see from Equation (24) that the even and odd trajectories are completely decoupled in the linearized system.

Performing the eigenvalue analysis for staggered u demonstrates the impact on stability of staggering the fourth coordinate. In particular, we find that one of the parasitic roots is eliminated, yielding four principle roots at $\lambda = +1$ and three parasitic roots at $\lambda = -1$. Staggering u thus reduces the possibility for instability. Note that the staggering was only made possible by the lack of dependence of the guiding center Lagrangian on $\dot{u}$.

The most important consideration is whether the parasitic modes are stable or unstable. The above analysis shows the modes to be marginally stable for the variational midpoint algorithm. Backward error analysis may be performed to derive vector fields governing the parasitic mode behavior [1, 24], but the analysis for nonlinear stability can be complicated.

14

Empirically, we find the modes to be weakly unstable - growing to detrimental amplitudes after several hundred or thousand toroidal transits.

Given the weak instability of the parasitic modes, the initial amplitude of the undesired modes is an important factor in determining the overall impact on the numerical fidelity. As might be expected, the initial amplitude of the parasitic modes is determined by the full set of initial conditions; for a k-step numerical method applied to a first order ODE, there are $k-1$ excess initial conditions and $k-1$ parasitic roots. Careful initialization of the system has a strong impact on the numerical fidelity of the variational midpoint guiding center algorithm.

2. Initial Conditions

To initialize the parasitic modes to minimum amplitude, backward error analysis guides a particular starting procedure [1, 24, 26]. Typically, the k initial conditions required to iterate a k-step method are provided by (i) the initial value problem and (ii) accurate approximations to the true solution. That is, if X_H is the vector field specifying the ODE and ϕ_t its flow map, the conventional starting procedure selects $\mathbf{z}_0$ as given, $\mathbf{z}_1 = \phi_h(\mathbf{z}_0), ..., \mathbf{z}_k = \phi_h^k(\mathbf{z}_0)$, where an accurate one-step method is used to approximate ϕ_h.

Alternatively, one can determine a "modified vector field" governing the dynamics of the principle mode. By sampling initial conditions along the flow of the vector field describing the smooth behavior, the parasitic modes can be reduced to initial amplitudes scaling with large powers of the step size h. A sketch contrasting the starting procedures is provided in Fig. (1).To determine the modified vector field, consider the flow of the principle mode, denoted $\widetilde{\varphi}_t$, defined by:

$$D_2 L_d(z_0, \widetilde{\varphi}_h(z_0)) + D_1 L_d(\widetilde{\varphi}_h(z_0), \widetilde{\varphi}_{2h}(z_0)) = 0. \tag{26}$$

Constraining the dependence of the flow to a single position z_0 restricts the dynamics to the original space and precludes the possibility of parasitic mode behavior. Next, the backward error ansatz assumes $\widetilde{\varphi}_t$ obeys:

$$\frac{d\widetilde{\varphi}_t}{dt} = \widetilde{X} = X_0 + hX_1 + h^2 X_2 + ... \tag{27}$$

The X_i may be iteratively determined by expanding Equation (26) about the initial time $t = 0$. Letting $\pounds_X$ denote the Lie derivative with respect to the vector field X, the expansion
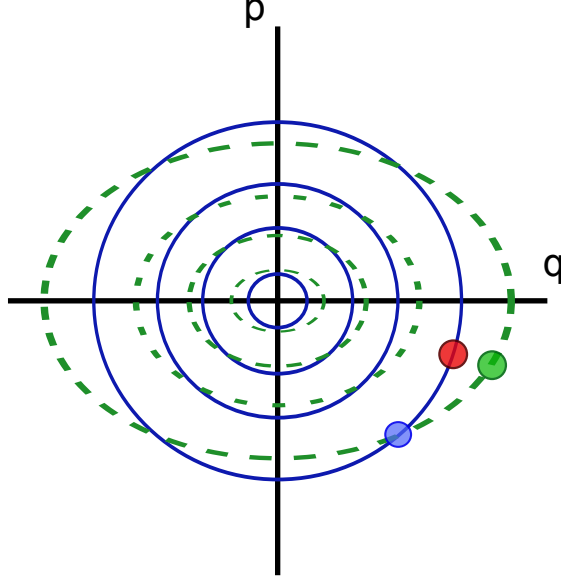
FIG. 1. Phase space portrait illustrating the standard starting procedure (red) and backward error initialization procedure (green). Blue curves represent integral curves of the continuous Hamiltonian vector field X_H, while green dashed curves represent integral curves of the modified vector field $\widetilde{X}$. An initial condition $\mathbf{z}_0$ is specified by the initial value problem, and depicted in the figure as the blue circle. The standard selection of $\mathbf{z}_1$ approximates the flow of the original vector field, depicted in red; while the backward error initial conditions selects $\mathbf{z}_1$ along the flow of the modified vector field, depicted in green.

takes the form:

$$
\begin{aligned}
\Big[h^0 \left(d_2 L_d(z_0, z_1) + d_1 L_d(z_1, z_2) \right) + \\
h^1 \left(\mathcal{L}_{(0,\widetilde{X})} d_2 L_d(z_0, z_1) + \mathcal{L}_{(\widetilde{X},2\widetilde{X})} d_1 L_d(z_1, z_2) \right) + \\
h^2 \left(\mathcal{L}_{(0,\widetilde{X})} \mathcal{L}_{(0,\widetilde{X})} d_2 L_d(z_0, z_1) + \mathcal{L}_{(\widetilde{X},2\widetilde{X})} \mathcal{L}_{(\widetilde{X},2\widetilde{X})} d_1 L_d(z_1, z_2) \right) \\
+ \ldots \Big]_{z_2 = z_1 = z_0} = 0.
\end{aligned}
\tag{28}
$$

Here, d_i denotes exterior derivative with respect to the i-th argument. To determine X_i, collect the preceding expression in powers of h and set to zero. For the midpoint discrete Lagrangian Equation (21), the h^0 and h^1 terms dictate $X_0 = X_H$ as expected for a consistent algorithm. Moreover, the symmetry of the midpoint discrete Lagrangian implies X_i is zero for all odd i. In general, the h^p term specifies the X_{p-1} vector field in terms of lower-order vector fields, the Hamiltonian, and derivatives of these quantities.
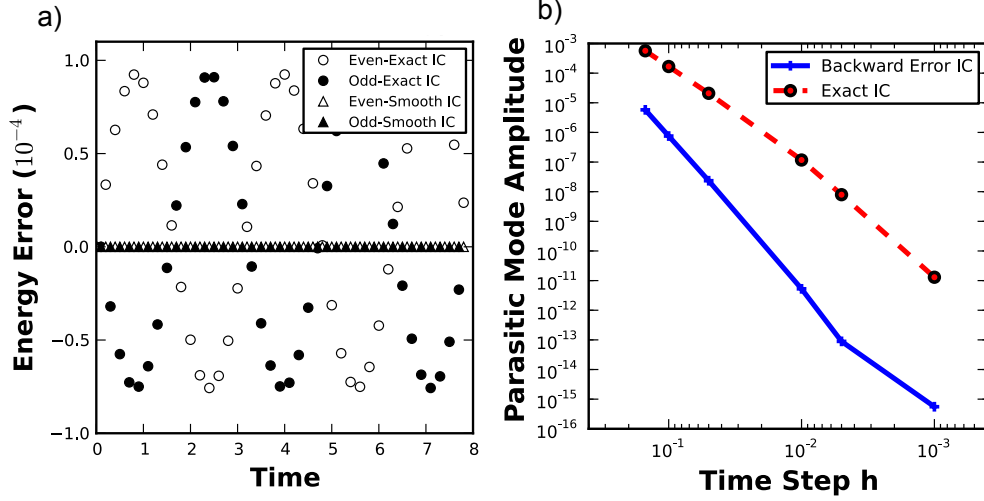
FIG. 2. Demonstration of reduced parasitic mode amplitude by backward error initialization. A single non-zero correction term is retained in the modified vector field at order h^2. **a)** Energy of a guiding center particle in straight magnetic field and harmonic potential. The trajectory initialized with the true solution (circles) exhibits a prominent even-odd oscillation in the energy, while the backward error initialized trajectory (triangles) is significantly smoother. **b)** Scaling of parasitic mode amplitude with true solution initialization and backward error initialization.

The parasitic mode amplitude reduction caused by backward error initialization is demonstrated in Fig. (2). For a simple test case, a guiding center particle is initialized in a straight magnetic field $\mathbf{B} = \hat{\mathbf{z}}$ and quadratic electric potential $\phi = z^2/2$. Initial conditions are sampled first along the flow of the original vector field X_H and secondly along the modified vector field $\widetilde{X}$ truncated after X_2. The mode-amplitude reduction is directly apparent in the numerical energy, and a scan in numerical step size indicates the backward error initialized parasitic mode scales with h^5 while the true-solution initialized mode scales with h^3. The step size scalings are a consequence of the level of agreement between the vector field used to generate the initial conditions and the modified vector field Equation (27).

3. Conservation Properties

In addition to stability considerations, the multistep aspect of the variational guiding center algorithms complicates the interpretation of the conserved quantities. As stated at the beginning of the section, the most natural notion of a symplectic guiding center

17

algorithm is a numerical time advance preserving the guiding center symplectic structure. Unfortunately, the multistep dynamics preserve a structure on a larger dimensional space than the physical dynamics. The excellent long-term behavior is then a surprising feature of the variational midpoint algorithm Equation (22). To explain the observed long-term numerical fidelity, we demonstrate that the *principle* mode preserves a two-form on the original space. The presence of a preserved structure is an indication that the long-term dynamics will behave well provided the parasitic modes remain small.

First, we analyze the symplectic structure preserved by the multistep variational midpoint algorithm Equation (22). Calculation of a preserved two-form is facilitated by the discrete variational principle, and has been performed for variational integrators in several References [10, 15, 17]. The calculation proceeds as follows. In contrast to the discrete action of Equation (18), which acts on arbitrary discrete trajectories $\{\mathbf{z}_k\}_{k=0}^{N}$, consider the *restricted* discrete action, $\bar{S}_d$, which acts on discrete paths satisfying the discrete Euler-Lagrange equations:

$$\bar{S}_d(\mathbf{z}_0, \mathbf{z}_1) = \sum_{k=0}^{N} L_d\left(\varphi_{kh}(\mathbf{z}_0, \mathbf{z}_1)\right) = \sum_{k=0}^{N} \left(\varphi_{kh}^* L_d\right)(\mathbf{z}_0, \mathbf{z}_1). \tag{29}$$

Here, $\varphi_h(\mathbf{z}_{k-1}, \mathbf{z}_k) = (\mathbf{z}_k, \mathbf{z}_{k+1})$ according to Equation (19). An exterior derivative of the restricted action yields:

$$d\bar{S}_d(\mathbf{z}_0, \mathbf{z}_1) = d_1 L_d(\mathbf{z}_0, \mathbf{z}_1) + \left(\varphi_{(N-1)h}^* d_2 L_d\right)(\mathbf{z}_0, \mathbf{z}_1). \tag{30}$$

All other terms in the summation vanish because the discrete trajectories satisfies the discrete Euler-Lagrange equations. An additional exterior derivative together with $d^2 = 0$ obtains the desired result:

$$\varphi_{(N-1)h}^* d_1 d_2 L_d(\mathbf{z}_0, \mathbf{z}_1) = d_1 d_2 L_d(\mathbf{z}_0, \mathbf{z}_1). \tag{31}$$

That is, φ_h is symplectic with discrete symplectic structure Ω_d given in coordinates by:

$$\Omega_d = \frac{\partial^2 L_d}{\partial z_0^i \partial z_1^j} dz_0^i \wedge dz_1^j. \tag{32}$$

The discrete symplectic structure Ω_d may be calculated for particular choices of discrete Lagrangian according to Equation (32). For the purposes of this discussion, the significant feature of Equation (32) is that Ω_d is defined on a space *twice* as large as that on which

18

continuous dynamics occur. Using the notation of Section (III B 1), the continuous guiding center symplectic structure has the form $\Omega = \vartheta_{i,j} dz^i \wedge dz^j$; it is defined on a four-dimensional space. In contrast, Ω_d is defined on an eight-dimensional space, according to Equation (32). This discrepancy explains the possibility of divergent parasitic modes despite constructing a structure-preserving algorithm from the onset. In particular, the bounded energy error obtained via backward error analysis for symplectic algorithms is not directly applicable to the multistep variational algorithms constructed by discretizing the phase-space action principle.

Despite the discouraging result of the preceding calculation, the excellent long-term numerical fidelity observed in variational guiding center algorithms suggests that the numerical dynamics behave well when the parasitic modes are not prominent. For the selection of stable initial conditions, we supposed a map $\widetilde{\varphi}_h$ that acted directly on the original dynamical space, as defined in Equation (26). Indeed, such a map has played an important role in the analysis of multistep methods, referred to as the "underlying one-step method" [27]. For the long-term assessment of the principle mode of the variational midpoint algorithm, it is the conservation properties of $\widetilde{\varphi}_h$ that are of interest.

The conservation properties of the underlying one-step method $\widetilde{\varphi}_h$ are similarly calculated by restricting the discrete action to act on paths generated by the map $\widetilde{\varphi}_h$. The procedure does not substantially differ than the multistep calculation, and the resulting discrete symplectic structure $\widetilde{\Omega}_d$ is given by:

$$\widetilde{\Omega}_d = \left(\frac{\partial^2 L_d}{\partial z_0^i \partial z_1^j} \right)_{(\mathbf{z}_0, \mathbf{z}_1) = (\mathbf{z}, \widetilde{\varphi}_h(\mathbf{z}))} \left(\widetilde{\varphi}_h^j \right)_{,k} dz^i \wedge dz^k. \tag{33}$$

As an explicit representation of $\widetilde{\varphi}_h$ is not known for non-zero h, it is difficult to represent $\widetilde{\Omega}_d$ directly in terms of known quantities for the midpoint discrete Lagrangian Equation (21). However, in the limit $h \to 0$, $\widetilde{\varphi}_0$ is the identity map and $\widetilde{\Omega}_d$ reduces to the continuous symplectic structure. Most significantly, the symplectic structure $\widetilde{\Omega}_d$ resides on a four-dimensional space even for finite h.

Overall, the symplecticity of the underlying one-step method $\widetilde{\varphi}_h$ with respect to $\widetilde{\Omega}_d$ is a moderately encouraging result. For nonzero h, the discrete two-form differs from that of the continuous dynamics. However, the principle mode behavior is Hamiltonian, converging to the original in the zero step size limit. While the sense in which it is a nearby Hamiltonian system differs from the conventional notion of symplectic integrators, the long-term numer-

ical behavior of the variational midpoint algorithm suggests that the preservation of $\widetilde{\Omega}_d$ is effective for constraining the numerical dynamics to remain close to the true dynamics.

C. Equilibrium Interfaces

The final practical consideration for implementing variational guiding center algorithms is the need to extract the magnetic vector potential from experimental equilibria. As an experimentally-relevant test case, we have interfaced the guiding center code with the EFIT equilibrium solver [28]. The ability to model test particles in experimentally determined equilibria is an important progression from previous studies in which the fields were analytically prescribed by a known vector potential [14, 15, 17]. The calculation of particle trajectories in experimental apparatus requires interfacing with magnetic fields specified at discrete locations on a numerical grid.

In the case of EFIT, the magnetic geometry of an experimental tokamak discharge is represented by the poloidal flux ψ on a two-dimensional spatial grid and a poloidal current function F on a flux grid. That is, the EFIT output specifies $\psi(R_i, z_j)$ and $F(\psi_i)$, where (R, z, θ) are cylindrical coordinates and indices identify points on the numerical grid. From these quantities, the magnetic field may be determined according to:

$$\mathbf{B} = \frac{1}{R} \left(\left(-\psi_{,z} \right) \hat{\mathbf{r}} + F \hat{\theta} + \psi_{,R} \hat{\mathbf{z}} \right). \tag{34}$$

For evaluation of the magnetic field at arbitrary position, one must interpolate $F(\psi(R, z))$ and $\nabla \psi(R, z)$ to the location of interest.

To model the guiding center equations of motion with the variational midpoint algorithm Equation (22), a vector potential must be determined that yields the magnetic geometry in Equation (34). As in Reference [29], we determine a vector potential by selecting a gauge for $\mathbf{A}$ and integrating the magnetic field the determine the unknown functions. Specifically, suppose a vector potential of the form:

$$\mathbf{A} = \psi \, \mathbf{d}\theta + A_z \, \mathbf{d}z. \tag{35}$$

The magnetic field is calculated according to:

$$\mathbf{B} = d\mathbf{A} = \psi_{,R} \, \mathbf{d}R \wedge \mathbf{d}\theta + \psi_{,z} \, \mathbf{d}z \wedge \mathbf{d}\theta + A_{z,R} \, \mathbf{d}R \wedge \mathbf{d}z. \tag{36}$$

Accounting for the metric tensor and matching components, the vector potential yields the magnetic field of Equation (34) if:

$$A_{z,R} = -\frac{F}{R}.$$ (37)

Construction of the magnetic vector potential then consists of the following steps: First, represent $\psi(R, z)$ using bicubic splines. Second, evaluate $F(\psi(R_i, z_j))$ on the grid and represent $F/R(R, z)$ using bicubic splines. Third, integrate to determine $A_z(R, z) = \int_0^R \frac{F(R', z)}{R'} dR'$. The vector potential can then be interpolated to any location in the domain for evaluation in the variational midpoint algorithm. The additional magnetic field quantities are derived from the interpolating polynomial of the vector potential. As a final note, the variational midpoint algorithm is implemented in three cylindrical dimensions; the axisymmetry of the magnetic geometry is not assumed at any point even though EFIT yields axisymmetric configurations.

IV. RESULTS

Now that the context, formal properties, and practical considerations of the variational guiding center algorithms have been established, we turn to the numerical results. This section presents the variational algorithm's performance in analytic and experimental equilibria and shows time to solution improvements for large numbers of particles using GPGPU hardware.

A. Analytic Axisymmetric Tokamak

As an initial test case, we consider a simple analytic toroidal geometry given by:

$$\mathbf{A} = \frac{B_0 R_0 z}{2R}\mathbf{d}R + \frac{B_0 r^2}{2q}\mathbf{d}\theta - \log(\frac{R}{R_0})\frac{B_0 R_0}{2}\mathbf{d}z,$$ (38)

where B_0, R_0 are constants, q is the safety factor and $r = \sqrt{z^2 + (R - R_0)^2}$ the minor radius. This field was used for the test case in Reference [15], but the present study differs in the choice of discrete Lagrangian and by tracking the full four-dimensional motion in (R, θ, z, u).

The results of a trapped particle with $B_0 = 1\,\mathrm{T}$, $R_0 = 1\,\mathrm{m}$, and $q = \sqrt{2}$ are shown in Fig. (3). The orbit fidelity of the $2\,\mathrm{keV}$ ion degrades substantially using the Runge-Kutta algorithm, despite the higher order local accuracy of the method. It is interesting to note that

the energy error at the end of the simulation is actually *less* for Runge-Kutta by about 30%; the Runge-Kutta integration slowly accumulates a fractional energy error of 7×10^{-4} while the variational midpoint algorithm exhibits periodic oscillations in energy with a maximum fractional error of 1×10^{-3}.
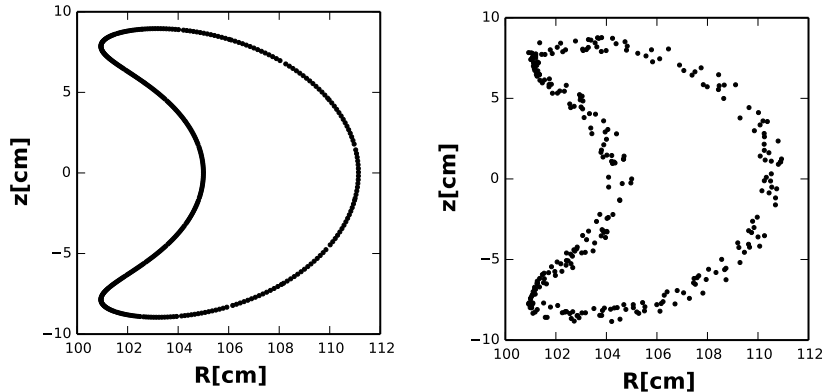

FIG. 3. Comparison of variational midpoint algorithm (left) and fourth-order Runge-Kutta (right) for the integration of a trapped particle trajectory. Particle is a 2 keV ion with initial state $(R, \theta, z, u) = (1.05 \, \text{m}, 0 \, \text{rad}, 0 \, \text{m}, 1.3 \times 10^5 \, \text{m s}^{-1})$. Numerical step size is $h = 12 \, \mu\text{s}$ and total run time is $3.6 \, \text{s}$.

B. Experimental Tokamak Equilibria

To demonstrate practical relevance of the variational guiding center algorithms, the guiding center test particle code has been interfaced with the EFIT magnetic equilibrium code. While interpolated magnetic fields do not formally differ from concise global analytic expressions, several practical considerations arise as detailed in Section III C.

For a test case, we have simulated a 10 keV ion in an experimentally determined equilibrium from the National Spherical Tokamak Experiment (NSTX). Shown in Fig. (4) is a sample trapped particle trajectory and convergence test in numerical step size. The spatial trajectory remains tighter for the variational algorithm than the Runge-Kutta algorithm of same order. Convergence of the variational algorithm to an accurate short-time simulation demonstrates successful construction of the magnetic vector potential necessary for Equation (22).
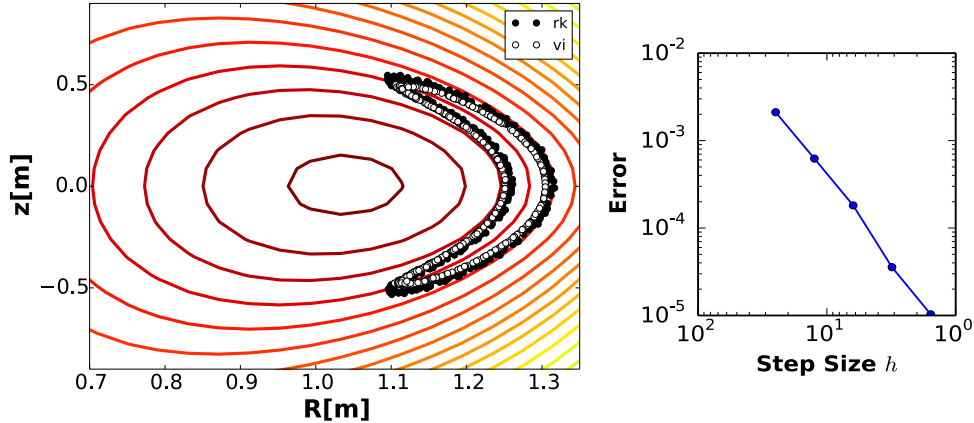
FIG. 4. Sample trapped particle trajectory using a 10 keV ion in an NSTX EFIT equilibrium over 2000 bounce times. **Left)** Overlay of second-order Runge-Kutta (blue) and second-order variational midpoint guiding center algorithms (green). **Right)** Convergence of variational midpoint trajectory to an accurate short-time Runge-Kutta trajectory.

It is interesting to note that the test particles drift in the EFIT magnetic geometry represented using bicubic splines. As the numerical step size decreases, the trajectories increasingly approximate closed orbits. However, the local error of the algorithm allows particles to sample magnetic geometry away from their trajectory, resulting in an overall drift. Given this fact, improvements in the variational calculations may be gained by using a smoother representation of the magnetic field [9] or by constructing higher-order variational algorithms.

C. GPGPU Parallelization

In conjunction with algorithmic advances, innovations in computational hardware may be leveraged to improve guiding center test particle calculations. Given the increasing prevalence of general-purpose graphics processing units (GPGPUs) at high performance computing facilities, parallelizing test particle codes to utilize such hardware can significantly reduce the run time for a given problem. The lack of interaction among drifting test particles simplifies the difficulty of parallelization, and motivates the investment of time to use highly parellel resources.

Using the CUDA progamming language, we have implemented a parallel driver for the
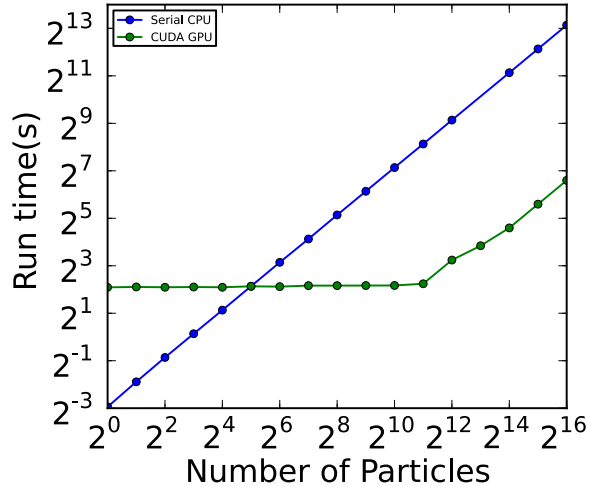
23

FIG. 5. Run time in seconds as a function of number of particles for a single core 2.5 GHz AMD Opteron CPU (**blue**) and a 2496 core nVidia Tesla k20m card (**green**).

guiding center test particle code. The run time as a function of the number of particles is shown in Fig. (5), where comparison is made between using the serial driver on a single 2.5 GHz CPU core and the CUDA driver on a 2496 core nVidia Tesla k20m GPGPU. For small numbers of particles, the CPU is faster by a factor of approximately 16. As the number of particles increases, the GPGPU becomes the more efficient hardware for the task. For large numbers of particles, the GPGPU is approximately 100 times faster than the single core CPU.

The strong performance of the GPU should be considered within the broader perspective of computing hardware. That is, nearly all CPU computing nodes possess more than a single core for use. A more "fair" comparison might compare the run time between a 16 core CPU and the GPU device. Extrapolating the preceding results, we would find use of the GPU device remains advantageous with a run time improvement factor of approximately six.

V. CONCLUSION

In summary, this work has improved the practical relevance of variational guiding center algorithms by interfacing with a magnetic equilibrium code and parallelizing the calculation for use on GPGPU devices. The magnetic vector potential was successfully constructed

24

from the discrete magnetic field data, and parallel calculations scaled well to large numbers of particles.

Additionally, the formal conservation properties of the algorithms and stability considerations have been thoroughly discussed. While the motivating application centered on guiding center test particle calculations, the discussion of multistep variational methods is pertinent to the broader class of phase-space Lagrangians. As long as the parasitic modes remain at small amplitude, variational discretizations of action principles in phase-space yield algorithms exhibiting desirable long-term features. Of course, it would be desirable to construct non-canonical structure-preserving algorithms which either preclude the possibility of parasitic modes or ensure the unphysical modes are damped, but such an endeavor remains for future work.

For the guiding center system, an important next step is to incorporate collisional effects in the numerical test-particle dynamics. While fast particles such as fusion alphas and runaway electrons may be approximated as collisionless over short time scales, collisions inevitably play an important role over longer time scales. For non-dissipative stochastic effects, such as a pitch-angle scattering event, it is likely the system may be formulated as a stochastic Hamiltonian system [30, 31] and stochastic variational integrators constructed by discretizing the corresponding action principle [32, 33]. For dissipative effects, including polarization drag, the non-Hamiltonian dynamics may still be formulated (and discretized) as an action extremization condition by using a Lagrange-d'Alembert variational principle [10]. The potential benefits of such constructions for the time evolution of fusion-relevant fast particle distributions are an interesting prospect.

Overall, variational integration and, more generally, geometric integration are promising approaches for performing high-fidelity guiding center test particle calculations. The authors are grateful to J. W. Burby and M. Kraus for helpful discussions on Hamiltonian systems and variational integrators. Similarly, we would like to thank N. Logan and S. Hudson for assistance with the EFIT equilibrium code. This work was performed under DOE contract DE-AC02-09CH11466.

[1] E. Hairer, C. Lubich, and G. Wanner. *Geometric Numerical Integration*. Springer, 2006.

[2] R. G. Littlejohn. Variational principles of guiding centre motion. *Journal of Plasma Physics*,

29(01):111–125, 1983.

[3] J. R. Cary and Alain J. Brizard. Hamiltonian theory of guiding-center motion. *Reviews of Modern Physics*, 81(02):693, 2009.

[4] R. Abraham and J. E. Marsden. *Foundations of Mechanics*. Addison-Wesley Publishing Company, 1987.

[5] J. E. Marsden and T. S. Ratiu. *Introduction to Mechanics and Symmetry*. Springer Science and Business Media, 1999.

[6] B. Karasözen. Poisson integrators. *Mathematical and Computer Modelling*, 40:1225–1244, 2004.

[7] R. B. White and M. S. Chance. Hamiltonian guiding center drift orbit calculation for plasmas of arbitrary cross section. *Physics of Fluids*, 27(10):2455, 1984.

[8] R. White and L. E. Zakharov. Hamiltonian guiding center equations in toroidal magnetic configurations. *Physics of Plasmas*, 10(3):573, 2003.

[9] D. Pfefferlé, J. P. Graves, W. A. Cooper, C. Misev, I. T. Chapman, and M. Turnyanskly ans S Sangaroon. NBI fast ion confinement in the helical core of MAST hybrid-like plasmas. *Nuclear Fusion*, 54:064020, 2014.

[10] J. E. Marsden and M. West. Discrete mechanics and variational integrators. *Acta Numerica*, pages 1–158, 2001.

[11] M. Leok and T. Shingel. Prolongation-collocation variational integrators. *IMA Journal of Numerical Analysis*, 32:1194–1216, 2011.

[12] M. Leok and T. Shingel. General techniques for constructing variational integrators. *Frontiers of Mathematics in China*, 7:273–303, 2012.

[13] J. Hall and M. Leok. Spectral variational integrators. *arXiv*, arXiv:1211.4534, 2012.

[14] H. Qin and X. Guan. Variational symplectic integrator for long-time simulations of the guiding-center motion of charged particles in general magnetic fields. *Physical Review Letters*, 100(3):035006, 2008.

[15] H. Qin, X. Guan, and W. M. Tang. Variational symplectic algorithm for guiding center dynamics and its application in tokamak geometry. *Physics of Plasmas*, 16(04):042510, 2009.

[16] J. Li, H. Qin, Z. Pu, L. Xie, and S. Fu. Variational symplectic algorithm for guiding center dynamics in the inner magnetosphere. *Physics of Plasmas*, 18(05):052902, 2011.

[17] J. Squire, H. Qin, and W. M. Tang. Gauge properties of the guiding center variational

symplectic integrator. *Physics of Plasmas*, 19(05):052501, 2012.

[18] M. Kraus. Variational integrators in plasma physics, 2013.

[19] V. I. Arnold. *Mathematical Methods of Classical Mechanics*. Springer, 1989.

[20] J. E. Marsden and T. S. Ratiu. *Introduction to Mechanics and Symmetry*. Springer Science and Business Media, 1999.

[21] T. Frankel. *The Geometry of Physics: An Introduction*. Cambridge University Press, third edition, 2012.

[22] J. R. Cary and R. G. Littlejohn. Noncanonical Hamiltonian mechanics and its application to magnetic field line flow. *Annals of Physics*, 151:1–34, 1983.

[23] E. Hairer. Backward error analysis for multistep methods. *Numerische Mathematik*, 84:199–232, 1999.

[24] E. Hairer and C. Lubich. Symmetric multistep methods over long times. *Numerische Mathematik*, 97:699–723, 2004.

[25] Y.-F. Tang. The symplecticity of multi-step methods. *Computers Math. Applic.*, 1993.

[26] R. D'Ambrosio and E. Hairer. Long-term stability of multi-value methods for ordinary differential equations. *Journal of Scientific Computing*, 2014.

[27] U. Kirchgraber. Multi-step methods are essentially one-step methods. *Numerische Methematik*, 48:85–90, 1986.

[28] L.L. Lao, H. St. John, R. D. Stambaugh, and W. Pfeiffer. Separation of $\bar{\beta}_p$ and l_i in tokamaks of non-circular cross-section. *Nuclear Fusion*, 25(10):1421, 1985.

[29] J. M. Finn and L. Chacón. Volume preserving integrators for solenoidal fields on a grid. *Physics of Plasmas*, 12:054503, 2005.

[30] J.-A. Lázaro-Camí and J.-P. Ortega. Stochastic hamiltonian dynamical systems. *Reports on Mathematical Physics*, 61(1):65–122, 2008.

[31] J. W. Burby and H. Qin A. I. Zhmoginov. Hamiltonian mechanics of stochastic acceleration. *Physical Review Letters*, 111(19):195001, 2013.

[32] N. Bou-Rabee and H. Owhadi. Stochastic variational integrators. *IMA Journal of Numerical Analysis*, 29(2):421, 2008.

[33] N. Bou-Rabee and H. Owhadi. Long-run accuracy of variational integrators in the stochastic context. *SIAM Journal of Numerical Analysis*, 48(2):278–297, 2010.

Princeton Plasma Physics Laboratory
Office of Reports and Publications

Managed by
Princeton University

under contract with the
U.S. Department of Energy
(DE-AC02-09CH11466)